Chemisorption of CO_2 on Nickel Surfaces

Sheng-Guang Wang,[†] Dong-Bo Cao,[†] Yong-Wang Li,[†] Jianguo Wang,[†] and Haijun Jiao*[,†,‡]

State Key Laboratory of Coal Conversion, Institute of Coal Chemistry, Chinese Academy of Sciences, Taiyuan, Shanxi 030001, People's Republic of China, and Leibniz-Institut für Organische Katalyse an der Universität Rostock e.V. Albert-Einstein-Strasse, 29a, 18059 Rostock, Germany

Received: May 6, 2005; In Final Form: August 12, 2005

CO_2 chemisorption on the Ni(111), Ni(100), and Ni(110) surfaces was investigated at the level of density functional theory. It was found that the ability of CO_2 chemisorption is in the order of Ni(110) > Ni(100) > Ni(111). CO_2 has exothermic chemisorption on Ni(110) and endothermic chemisorption on Ni(111), while it is thermally neutral on Ni(100). It is also found that there is no significant lateral interaction between the adsorbed CO_2 at $^1/_4$ monolayer (ML) coverage, while there is stronger repulsive interaction at $^1/_2$ ML. On all surfaces, the chemisorbed CO_2 is partially negatively charged, indicating the enhanced electron transfer, and the stronger the electron transfer, the stronger the C═O bond elongation. The bonding nature of the adsorbed CO_2 on nickel surfaces has been analyzed. The thermodynamics of CO_2 dissociative chemisorption, compared with CO and O adsorption, has been discussed, and the thermodynamic preference is in the sequence Ni(100) > Ni(111) > Ni(110).

Introduction

Synthesis gas ($CO + H_2$, syngas) is a key intermediate in chemical industry and may be responsible for ~60% of the investments of large-scale gas conversion plants based on natural gas.[1] There are mainly four ways to produce syngas from natural gas: (i) steam reforming (SMR, eq 1), (ii) dry reforming (DMR, eq 2), (iii) catalytic partial oxidation (POX, eq 3), and (iv) autothermal reforming (ATR, combination of eqs 1 and 3).

$$CH_4 + H_2O = CO + 3H_2 \quad (1)$$

$$CH_4 + CO_2 = 2CO + 2H_2 \quad (2)$$

$$2CH_4 + O_2 = 2CO + 4H_2 \quad (3)$$

SMR is mainly used in the present industrial production of syngas, but DMR is attractive because it can be employed at remote natural gas fields containing large amounts of CO_2 and areas where water is not available. Furthermore, DMR yields syngas with lower H_2/CO ratios, which is a preferable feedstock for the Fischer−Tropsch synthesis (FTS) of long-chain hydrocarbons.[2]

However, there are some constraints in DMR, for example, carbon deposition and high reaction temperatures. Although the first reaction mechanism of reforming reactions was proposed in 1967,[3] our current understanding of the reaction mechanism has been obtained during the past decade.[4−25] The mechanism of DMR is thought to be complex, and this is because there are many intermediates on the catalyst surfaces and each intermediate might have more than one adsorbed state.

It is generally accepted that CO_2 activation on transition metal surfaces is structure sensitive; that is, different surface structures have different activities. Bradford and Vannice[2] showed the structure sensitivity of CO_2 adsorption on some transition metal surfaces, for example, dissociatively on Fe(111) and Fe(100) but nondissociatively on Fe(110). CO_2 adsorption on nickel surfaces is also structure sensitive, for example, dissociative on Ni(110), nondissociative on Ni(111), and both dissociative and nondissociative on Ni(100).[26,27]

It has been reported that adsorbed CO_2 on metal surfaces has two states, a physisorbed linear state and a chemisorbed bent $CO_2^{\delta-}$ state.[28] The chemisorbed anionic species represents an intrinsic precursor for CO_2 dissociation into CO and oxygen on the Ni(100)[29] and Fe(111)[30] surfaces. On the basis of ab initio valance-bond theory calculations, Freund and Messmer[28] analyzed three coordination models of CO_2 on transition metal complexes and found that the bonding between the CO_2 moiety and the metal atom is best described as a $CO_2^{\delta-}$ anion interacting with a Ni atom. They ascribed the bending mechanism of the CO_2 moiety to the associated electron transfer from metal to CO_2. However, they have not calculated the full structure on a nickel surface. Choe et al. modeled the adsorption and dissociation reaction of CO_2 on Ni(111) by a 25-atom cluster by using the atom-superposition and electron-delocalization molecular orbital method.[31] The most stable state of CO_2 on Ni(111) was reported on the $\sigma_{(1)}$ site, that is, the bridge site with two oxygen atoms bonding with two surface nickel atoms, respectively. However, no detailed theoretical studies on CO_2 activation on the different nickel surfaces were reported. This paper presents the results of a theoretical study on CO_2 chemisorption on the Ni(111), Ni(100), and Ni(110) surfaces. The surface structure and energy as well as the net charge of the chemisorbed CO_2 have been analyzed systematically.

Methods and Models

Density functional theory calculations within the generalized gradient approximation (GGA)[32] and the Perdew−Burke−Ernzerhof (PBE)[33] functional were carried out to study CO_2 chemisorption on nickel surfaces. All calculations were carried out using the Cambridge sequential total energy package (CASTEP).[34] Ionic cores were described by the ultrasoft

* Corresponding author. E-mail: haijun.jiao@ifok-rostock.de.
[†] Chinese Academy of Sciences.
[‡] Leibniz-Institüt Organische Katalyse an der Universität Rostock e.V. Albert-Einstein-Strasse.

10.1021/jp052355g CCC: $30.25
Published on Web 09/16/2005

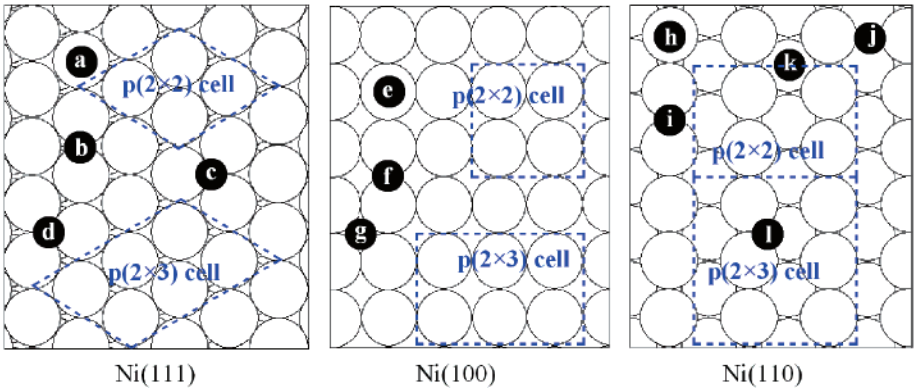

Figure 1. Top views of the nickel surfaces.

pseudopotential,[35] and the Kohn−Sham one-electron states were expanded in a plane wave basis set up to 340 eV. A Fermi smearing of 0.1 eV was utilized. Brillouin zone integration was approximated by a sum over special *k* points chosen using the Monhorst−Pack scheme.[36] The pseudopotential with a partial core was used in spin-polarized calculations to include nonlinear core corrections,[37] and spin polarization has a major effect on the adsorption energies for a magnetic system.[38−42] The vacuum between the slabs was set to span a range of 12 Å to ensure no significant interaction between the slabs. The convergence criteria for the structure optimization and energy calculation were set to (a) a self-consistent field (SCF) tolerance of 1.0×10^{-6} eV/atom, (b) an energy tolerance of 1.0×10^{-5} eV/atom, (c) a maximum force tolerance of 0.03 eV/Å, and (d) a maximum displacement tolerance of 1.0×10^{-3} Å. The bulk lattice constant and magnetic moment were calculated to test the method and convergence criteria employed. The computed lattice constant (3.54 Å) and magnetic moment (0.59 μ_B) with *k* points of $6 \times 6 \times 6$ agree well with the experiment (3.52 Å and 0.61 μ_B), and this validates the employed methods and models nicely for the nickel system.

The chemisorption energy per CO_2 molecule was defined as $\Delta E_{chem} = E(CO_2/slab) - [E(CO_2) + E(slab)]$, where the first term is the total energy for the slab with the chemisorbed CO_2 on the surface, the second term is the total energy of free CO_2, and the third term is the total energy of the bare slab of the surface. Therefore, a negative ΔE_{chem} value means exothermic chemisorption, and a positive ΔE_{chem} value means endothermic chemisorption. For CO_2 dissociation into CO and atomic oxygen on the surface, the dissociation energies are defined as the difference between the sum of adsorbed CO and O and the sum of bare slab and free CO_2, $\Delta E_{diss} = [E(CO/slab) + E(O/slab)] - [E(CO_2) + 2E(slab)]$. Therefore, a negative ΔE_{diss} value means exothermic dissociation, while a positive ΔE_{diss} value means endothermic dissociation.

Metal particles grown at high temperature on oxide or graphite substrates have polyhedral shapes exhibiting (111), (100), and (110) facets,[43] as shown in Figure 1. Therefore, these nickel facets were used to describe CO_2 chemisorption on nickel catalysts. First, three-layered models were used; the results were then validated using models with more layers. In all of our calculations, the nickel atoms of the top two layers were allowed to relax, while those in other layers were fixed for three-, four-, and five-layered models. The computed structural and energetic parameters were compared between the three-layered models and the average of three-, four-, and five-layered ones with the most stable chemisorption configurations on each surface. The differences are less than 0.001 Å for bond lengths and less than 0.01 eV for chemisorption energies. Therefore, the three-layered models with relaxation of the first two layers are reasonable and do not bias the results. The p(2 × 2) unit cell was used to model the $^1/_4$ and $^1/_2$ monolayer (ML) coverages, and this size was widely used in the previous theoretical investigation on molecule chemisorption on transition metal surfaces.[44−46] However, the p(2 × 3) unit cell was employed to model the $^1/_6$ ML coverage, as shown in Figure 1. To understand the bonding nature of adsorbed CO_2 on nickel surfaces, detailed analyses of electronic structure with local density of states (LDOS) were carried out.

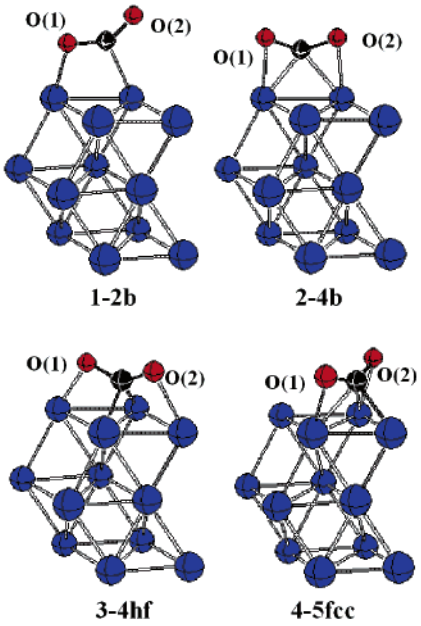

Figure 2. Structures of chemisorbed CO_2 on Ni(111) at $^1/_4$ ML coverage.

Results and Discussion

(a) CO_2 Chemisorption on Ni(111). Our calculation began with $^1/_4$ ML coverage, and the *k* point of $5 \times 5 \times 1$ Monkhorst−Pack meshes was used. From all possible orientations on Ni(111), only four stable surface structures were obtained (**1**−**4**, Figure 2). The computed adsorption energies, structural parameters, and net charges are listed in Table 1.

In **1-2b** (2-fold bridge site), CO_2 interacts with two adjacent Ni atoms via one C═O bond and forms one Ni−O and one Ni−C bond, and the C−O bonds are elongated compared to free CO_2 (1.262 and 1.203 Å vs 1.171 Å). In **2-4b** (4-fold bridge site), CO_2 interacts with two adjacent Ni atoms via two C═O bonds and forms two Ni−C bonds, each of the oxygen atoms

TABLE 1: Computed Chemisorption Energies (ΔE_{chem}, eV) per Molecule and Structures (d, Å and θ, deg) as Well as the Net Charges (q) of CO_2 on the Ni(111) Surface

	ML	ΔE_{chem}	$d_{O(1)-C}$	$d_{O(2)-C}$	$d_{O(1)-Ni}$	$d_{O(2)-Ni}$	d_{C-Ni}	θ_{OCO}	q	$q_{O(1)}$	$q_{O(2)}$	q_C
CO_2			1.171	1.171				180.0	0	−0.51	−0.51	1.02
1-2b	1/4	0.31	1.262	1.203	1.965		1.990	137.8	−0.42	−0.44	−0.40	0.42
2-4b	1/4	0.45	1.224	1.223	2.133	2.139	2.158, 2.132	142.6	−0.44	−0.40	−0.40	0.36
3-4hf	1/4	0.36	1.261	1.255	2.117	2.165	2.087, 1.986	134.7	−0.57	−0.42	−0.41	0.26
4-5fcc	1/4	0.46	1.253	1.251	2.154	2.091	2.252, 2.211, 1.981	133.2	−0.57	−0.42	−0.41	0.26
1-2b	1/6	0.26	1.265	1.208	1.976		1.971	136.6	−0.45	−0.46	−0.41	0.42
3-4hf	1/6	0.31	1.263	1.261	2.127	2.143	2.074, 1.980	133.6	−0.61	−0.43	−0.43	0.25

TABLE 2: Computed Chemisorption Energies (ΔE_{chem}, eV) per Molecule and Structures (d, Å and θ, deg) as Well as the Net Charges (q) of CO_2 on the Ni(100) Surface

	ML	ΔE_{chem}	$d_{O(1)-C}$	$d_{O(2)-C}$	$d_{O(1)-Ni}$	$d_{O(2)-Ni}$	d_{C-Ni}	θ_{OCO}	q	$q_{O(1)}$	$q_{O(2)}$	q_C
CO_2			1.171	1.171				180.0	0	−0.51	−0.51	1.02
5-3h	1/4	−0.08	1.264	1.257	2.008	2.027	1.902	130.6	−0.59	−0.44	−0.43	0.28
6-2b	1/4	0.07	1.256	1.206	1.961		1.968	138.5	−0.44	−0.45	−0.40	0.41
7-2lb	1/4	0.01	1.273	1.226	1.994		1.928	134.0	−0.59	−0.47	−0.40	0.28
6-2b(a)	1/2 (A)	0.35[a]	1.250	1.196	1.910		2.014	140.0	−0.34	−0.44	−0.38	0.48
	1/2 (B)		1.247	1.194	1.920		2.026	140.8	−0.32	−0.43	−0.38	0.49
5-3h	1/6	−0.14	1.268	1.259	1.994	2.032	1.896	129.6	−0.61	−0.45	−0.44	0.28

[a] The average value of the two co-chemisorbed CO_2 molecules on the p(2 × 2) surface model. (A) and (B) represent the two co-chemisorbed CO_2 molecules on the p(2 × 2) surface model, respectively.

forms one Ni—O bond, and the C—O bonds are elongated to 1.224 and 1.223 Å, respectively. In **3-4hf**, CO_2 interacts with four Ni atoms on the surface by occupying one face-centered cubic (fcc) site and one neighboring hexagonal-close-packed (hcp) site, the carbon center bridges the adjacent Ni atoms with the formation of two Ni—C bonds, and each of the oxygen atoms interacts with the trans angular Ni atoms. The C—O bonds in **3-4hf** are elongated to 1.261 and 1.255 Å. In **4-5fcc** (5-fold fcc site), CO_2 interacts with three Ni atoms on the fcc site and the C—O bonds are elongated to 1.253 and 1.251 Å. In addition, we have tried to locate the adsorption models with carbon at the top, but these configurations desorbed during the optimization. On Ni(111), the chemisorbed CO_2 moiety has a bent structure with an OCO angle of about 133−143° (Table 1).

As given in Table 1, all four structures have endothermic chemisorption energies, indicating that CO_2 chemisorption on Ni(111) is thermodynamically not favored. The most stable chemisorbed structure (**1-2b**) has an adsorption energy of 0.31 eV, while **2-4b**, **3-4hf**, and **4-5fcc** are less stable (0.45, 0.36, and 0.46 eV), respectively. However, our result disagrees with those of Choe et al. by using the semiempirical approach.[31] In their calculation, the most stable configuration was on the bridge site with two oxygen atoms binding with two surface nickel atoms, respectively. In our calculation, this configuration converges to **2-4b** during the geometrical optimization. However, there are no experimental data available for comparison with our calculated chemisorption energies.

Despite the disfavored endothermic chemisorption at 1/4 ML, we have studied CO_2 chemisorption on Ni(111) at 1/2 ML. However, no stable structures with two adsorbed CO_2 molecules at 1/2 ML were found. Structure optimization leads to the desorption and escape of one CO_2 molecule from the surface, indicating that it is impossible to get CO_2 adsorption on Ni(111) at coverages higher than 1/4 ML.

For testing the possible lateral interaction of the chemisorbed CO_2 at 1/4 ML coverage, a surface model with a 1/6 ML coverage and the k point of 3 × 5 × 1 Monkhorst−Pack meshes were employed. As at 1/4 ML, we chose the two most stable structures (**1-2b** and **3-4hf**) at 1/6 ML; the computed chemisorption energies are 0.26 and 0.31 eV, respectively, and they are 0.05 eV stronger (less endothermic) than those at 1/4 ML. It indicates that there is no significant lateral repulsion between the chemisorbed CO_2 at 1/4 ML, but chemisorption of CO_2 on Ni(111) at 1/6 ML is still not favored thermodynamically.

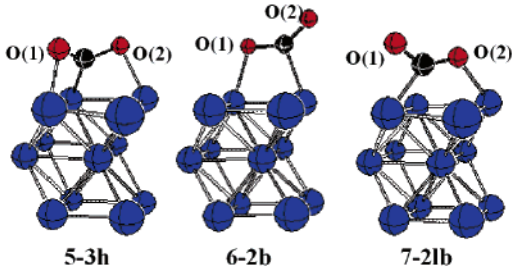

Figure 3. Structures of chemisorbed CO_2 on Ni(100) at 1/4 ML coverage.

Apart from the structure and energy, it is also interesting to look into the change of the charges. The net charge of the chemisorbed CO_2 on Ni(111) is given in Table 1, compared with those of free CO_2. It shows clearly that the chemisorbed CO_2 is partially negatively charged (−0.42 to −0.61), indicating electron transfer from the nickel surface into CO_2. Therefore, the best and most appropriated description of CO_2 on the surface should be $CO_2^{\delta-}$.

As the limited case of electron transfer, we have computed the radical anion of $CO_2^{\bullet-}$. As expected, the C—O bonds of $CO_2^{\bullet-}$ are elongated compared to CO_2 (1.236 Å vs 1.171 Å), and $CO_2^{\bullet-}$ has a bent structure with an OCO angle of 137.5°. Therefore, the bending mechanism of the partially negatively charged $CO_2^{\delta-}$ is due to the effect of electron transfer from the surface into the antibonding orbital of CO_2, as suggested by Freund and Messmer.[28]

(b) CO_2 Chemisorption on Ni(100). The calculation began with a 1/4 ML coverage, and the k point of 4 × 4 × 1 Monkhorst−Pack meshes was used. From all possible orientations on Ni(100), only three stable surface structures were found (**5**−**7**, Figure 3). The computed chemisorption energies, structural parameters, and net charges are listed in Table 2.

In **5-3h** (3-fold hollow site), CO_2 occupies a hollow site on the surface of three surface nickel atoms and the C—O bonds are elongated to 1.264 and 1.257 Å. In **6-2b** (2-fold bridge site), one of the C═O bonds interacts with two adjacent nickel atoms and the C—O bonds are elongated to 1.256 and 1.206 Å. In

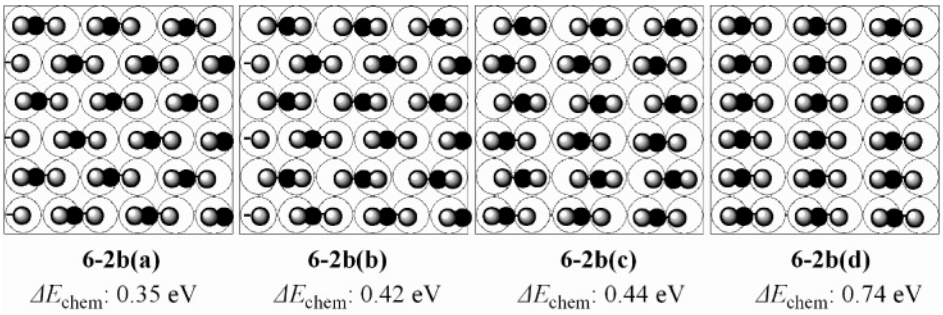

Figure 4. Top views of chemisorbed CO_2 on Ni(100) at $^1/_2$ ML coverage.

7-2lb (2-fold long-bridge site), one of the C═O bonds interacts with two trans angular nickel atoms and the C—O bonds are elongated to 1.273 and 1.226 Å. On Ni(100), the adsorbed CO_2 moiety has a bent structure with an OCO angle of about 131—139° (Table 2).

As given in Table 2, **5-3h** has a slightly exothermic chemisorption energy (−0.08 eV), while those of **6-2b** and **7-2lb** are slightly positive (0.07 and 0.01 eV, respectively). However, such small energies in magnitude indicate the rather thermally neutral chemisorption of CO_2 on Ni(100) at $^1/_4$ ML.

Using the same surface models at $^1/_4$ ML, we have studied CO_2 chemisorption on Ni(111) at $^1/_2$ ML. During the optimization process, the structures **5-3h** and **7-2lb** converged to **6-2b** from all initial orientations. As shown in Figure 4, there are four stable configurations on the basis of the relative orientation of the two adsorbed CO_2 molecules (**6-2b(a)**—**6-2b(d)**). The C—O bond lengths of **6-2b** are shorter than those at $^1/_4$ ML, indicating that the high coverage decreased the degree of activation of the chemisorbed $CO_2^{\delta-}$. The most stable configuration is **6-2b(a)**, in which the chemisorbed $CO_2^{\delta-}$ prefers to disperse and to minimize the repulsion. The chemisorption energy per molecule changed from −0.08 eV at $^1/_4$ ML to 0.35 eV at $^1/_2$ ML, and this means that the adsorption of the second CO_2 molecule costs 0.78 eV. Therefore, it is energetically not favorable to get higher CO_2 coverages.

For testing the possible lateral interaction of the chemisorbed CO_2 at a $^1/_4$ ML coverage, a surface model with a $^1/_6$ ML coverage and the *k* point of 3 × 4 × 1 Monkhorst—Pack meshes were employed. As at $^1/_4$ ML, we chose the most stable structure (**5-3h**) at $^1/_6$ ML, and the computed chemisorption energy is −0.14 eV, which is only 0.06 eV stronger (more exothermic) than that at $^1/_4$ ML. It indicates that there is no significant lateral repulsion between chemisorbed CO_2 molecules at $^1/_4$ ML.

(c) CO_2 Chemisorption on Ni(110). The calculation of CO_2 chemisorption on Ni(110) began with $^1/_4$ ML, and the *k* point of 3 × 4 × 1 Monkhorst—Pack meshes was used. From all possible orientations on Ni(110), only six stable structures were found (**8**—**13**, Figure 5). The computed chemisorption energies, structural parameters, and net charges are listed in Table 3.

In **8-3hu** (3-fold hollow-up site), CO_2 occupies a hollow site on the surface and binds with three top-layer nickel atoms and the C—O bonds are elongated to 1.271 and 1.268 Å. In **9-2b** (2-fold bridge site), CO_2 interacts with two adjacent top-layer Ni atoms via one C═O bond and forms one Ni—O and one Ni—C bond and the C—O bonds are elongated compared with free CO_2 (1.268 and 1.208 Å vs 1.171 Å). In **10-4b** (4-fold bridge site), CO_2 interacts with two adjacent top-layer Ni atoms via two C═O bonds and forms two Ni—C bonds, each of the oxygen atoms forms one Ni—O bond, and the C—O bonds are elongated to 1.231 and 1.230 Å, respectively. In **11-2lb** (2-fold long-bridge site), CO_2 interacts with two top-layer Ni atoms on adjacent ridges via one C═O bond and forms one Ni—O and one Ni—C bond and the C—O bonds are elongated to 1.249 and 1.230 Å. In **12-5h** (5-fold hollow site), CO_2 occupies a hollow site between two ridges and binds with four top-layer nickel atoms via two oxygen atoms, respectively, with one second-layer nickel atom via a carbon atom. The C—O bonds in **12-5h** are elongated to 1.292 and 1.291 Å. In **13-3h** (3-fold hollow site), CO_2 occupies a hollow site between two ridges and binds with two top-layer nickel atoms via two oxygen atoms, respectively, with a second-layer nickel atom via a carbon atom, and the C—O bonds in **13-3h** are elongated to 1.274 and 1.270 Å. On the Ni(110) surface, the chemisorbed CO_2 moiety has a bent structure with an OCO angle of about 123—141° (Table 3).

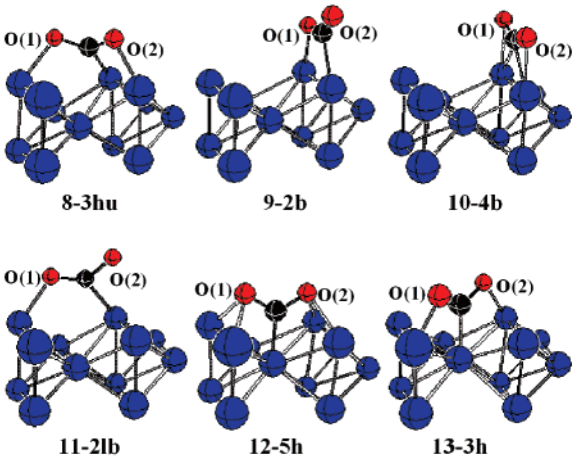

Figure 5. Structures of chemisorbed CO_2 on Ni(110) at $^1/_4$ ML coverage.

As given in Table 3, all chemisorption on Ni(110) is exothermic and favored thermodynamically. Structure **8-3hu** with an exothermic chemisorption energy of −0.39 eV is the most stable surface structure at $^1/_4$ ML, while other structures are less stable (−0.14 to −0.23 eV).

Since CO_2 chemisorption on Ni(110) at $^1/_4$ ML is exothermic, we are interested in the possibility for further CO_2 adsorption at $^1/_2$ ML. The optimized stable structures are shown in Figure 6, and the computed chemisorption energies, structural parameters, and net charges are listed in Table 3. On the basis of the relative orientation of the second CO_2 molecules, there are three stable surface structures for **8-3hu**, two for **10-4b**, four for **11-2lb**, and one for **12-5h**. However, no stable surface structures for **9-2b** and **13-3h** with two CO_2 molecules were found, and optimization leads all initial structures of **9-2b** into **10-4b** and **13-3h** into **8-3hu**, respectively.

Among these stable surface structures, the structure of dispersed **8-3hu(a)** is the most stable one with an exothermic chemisorption energy of −0.21 eV per CO_2 molecule. It is noteworthy that the chemisorption energy of **8-3hu** at $^1/_2$ ML

TABLE 3: Computed Chemisorption Energies (ΔE_{chem}, eV) per Molecule and Structures (d, Å and θ, deg) as Well as the Net Charges (q) of CO_2 on the Ni(110) Surface

	ML	ΔE_{chem}	$d_{O(1)-C}$	$d_{O(2)-C}$	$d_{O(1)-Ni}$	$d_{O(2)-Ni}$	d_{C-Ni}	θ_{OCO}	q	$q_{O(1)}$	$q_{O(2)}$	q_C
CO_2			1.171	1.171				180.0	0	−0.51	−0.51	1.02
8-3hu	1/4	−0.39	1.271	1.268	1.987	1.980	1.884	126.5	−0.65	−0.47	−0.48	0.30
9-2b	1/4	−0.21	1.268	1.208	1.909		1.926	136.4	−0.49	−0.47	−0.42	0.40
10-4b	1/4	−0.23	1.231	1.230	2.029	2.043	2.094, 2.016	141.3	−0.53	−0.43	−0.42	0.32
11-2lb	1/4	−0.22	1.249	1.230	1.967		1.889	136.5	−0.52	−0.48	−0.43	0.39
12-5h	1/4	−0.18	1.292	1.291	2.096, 2.081	2.087, 2.078	1.890	122.5	−0.74	−0.48	−0.49	0.23
13-3h	1/4	−0.14	1.274	1.270	1.978		1.956	125.2	−0.65	−0.46	−0.46	0.27
8-3hu(a)	1/2 (A)	−0.21[a]	1.260	1.253	1.961	2.023	1.927	130.2	−0.57	−0.44	−0.45	0.32
	1/2 (B)		1.258	1.252	1.965	2.035	1.936	130.8	−0.56	−0.43	−0.45	0.32
10-4b(a)	1/2 (A)	−0.25[a]	1.233	1.228	1.977	2.062	2.119, 1.973	141.6	−0.52	−0.42	−0.41	0.31
	1/2 (B)		1.233	1.228	1.977	2.060	2.119, 1.973	141.7	−0.52	−0.42	−0.41	0.31
11-2lb(a)	1/2 (A)	−0.14[a]	1.232	1.226	1.976	1.908	2.155	140.8	−0.44	−0.45	−0.41	0.42
	1/2 (B)		1.232	1.225	1.976	1.909	2.156	140.9	−0.44	−0.45	−0.41	0.42
12-5h(a)	1/2 (A)	0.25[a]	1.287	1.286	1.028, 1.026	1.026, 1.025	1.959	121.3	−0.75	−0.45	−0.45	0.15
	1/2 (B)		1.287	1.286	1.029, 1.027	1.026, 1.029	1.963	121.4	−0.75	−0.45	−0.45	0.15
8-3hu	1/6	−0.42	1.271	1.269	1.999	1.989	1.881	126.4	−0.67	−0.48	−0.49	0.30

[a] The average value of the two co-chemisorbed CO_2 molecules on the p(2 × 2) surface model. (A) and (B) represent the two co-chemisorbed CO_2 molecules on the p(2 × 2) surface model, respectively.

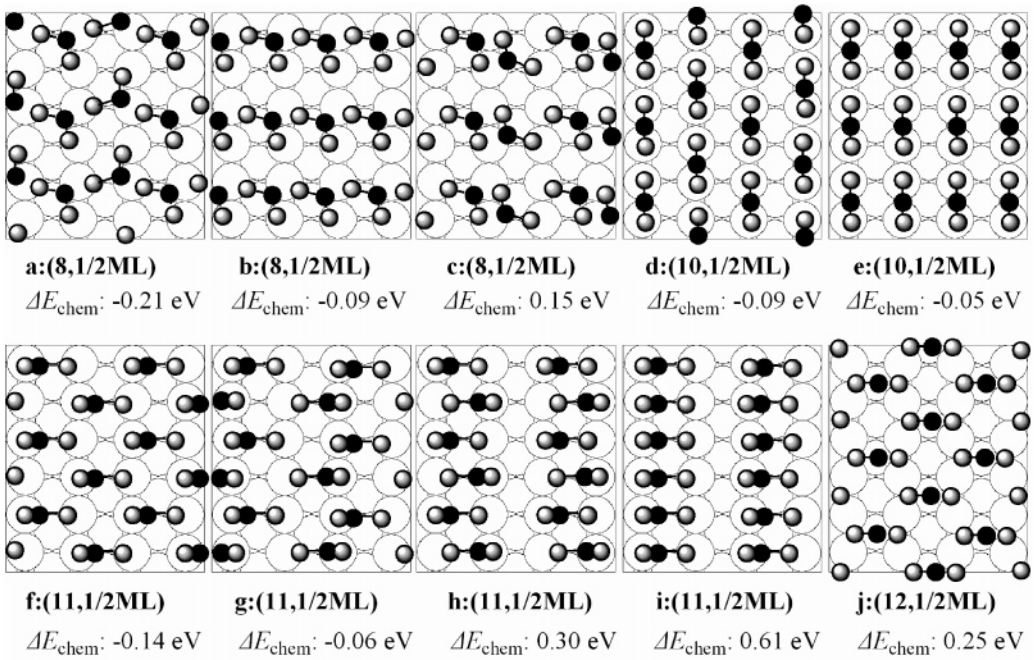

Figure 6. Top views of chemisorbed CO_2 on Ni(110) at 1/2 ML coverage.

is less negative (weaker) than that at 1/4 ML (−0.39 eV), indicating the repulsive interaction between the adsorbed CO_2 molecules.

For testing the possible lateral interaction of the chemisorbed CO_2 at a 1/4 ML coverage, a surface model with a 1/6 ML coverage and the k point of 3 × 3 × 1 Monkhorst−Pack meshes were used. As at 1/4 ML, we chose the most stable structure (**8-3hu**) at 1/6 ML; the computed chemisorption energy is −0.42 eV, and it is 0.03 eV stronger (more exothermic) than that at 1/4 ML. It indicates that there is no significant lateral repulsion between chemisorbed CO_2 molecules at 1/4 ML.

(d) Electronic Factor. To explain the electronic structures of the chemisorbed CO_2, the local density of states (LDOS) is computed. Since the LDOS of the chemisorbed CO_2 are similar on Ni(111), Ni(100), and Ni(110), only the most stable states on each surface at 1/4 ML are presented, that is, **1-2b**, **5-3h**, and **8-3hu**, respectively. As shown in Figure 7, the highest occupied molecular orbital (HOMO) of free CO_2 is $1\pi_g$, which is situated on oxygen atoms, while the lowest unoccupied molecular orbital (LUMO) is $2\pi_\mu$, which is the antibinding

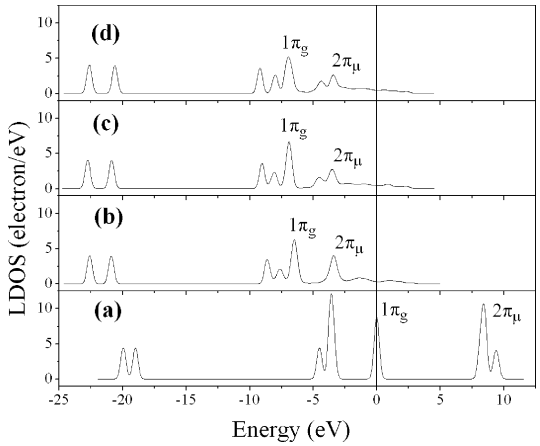

Figure 7. Local density of states of chemisorbed CO_2 on nickel surfaces at 1/4 ML coverage: (a) free CO_2; (b) **1-2b**; (c) **5-3h**; (d) **8-3hu**.

orbital of CO_2 situated on the carbon atom and two oxygen atoms. In the chemisorbed CO_2, the bands shift downward,

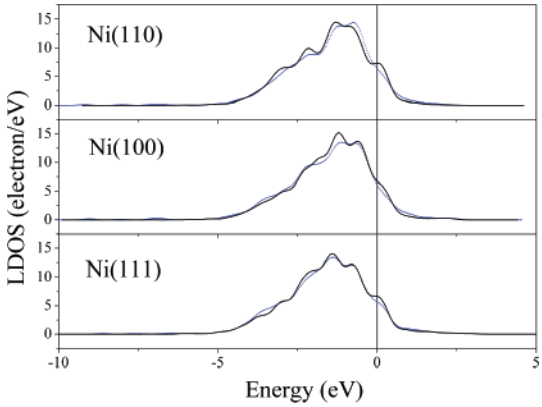

Figure 8. d-Band local density of states of the top layer of the nickel surfaces. The solid black lines and dashed blue lines represent before and after CO_2 chemisorption of **1-2b**, **5-3h**, and **8-3hu**, respectively.

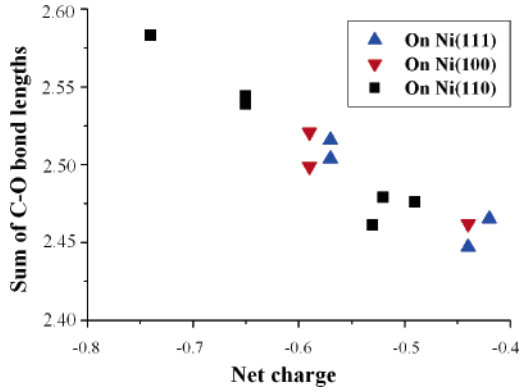

Figure 9. C−O bond lengths compared with the net charges of chemisorbed CO_2 at $^1/_4$ ML coverage.

which corresponds to the binding of CO_2 with the nickel surfaces. As a consequence of charge transfer (in a late section below), the antibonding $2\pi_\mu$ orbital falls below the Fermi level for the adsorbed cases and the intensity is also lowered considerably as compared to free CO_2. Further calculations on bent CO_2 show that the bending of CO_2 molecules will lower the intensity and the energy level of the LUMO. Therefore, both charge transfer and bending of CO_2 will activate CO_2 synergically.

For comparison, the LDOS of the three bare nickel surfaces are calculated. As shown in Figure 8, the frontier d orbitals of nickel surfaces are in broad form, and they are responsible for the electron transfer to the chemisorbed CO_2. In addition, it is interesting to note that the intensities of the occupied orbitals at the Fermi level of Ni(110), Ni(100), and Ni(111) are 8.0, 7.5, and 7.2 e/eV, respectively; this is in agreement with the order of chemisorption ability of Ni(110) > Ni(100) > Ni(111).

The net charge of the chemisorbed CO_2 on the Ni surface is given in Tables 1−3, compared with those of free CO_2. It shows clearly that the chemisorbed CO_2 molecules are partially negatively charged, indicating electron transfer from the nickel surface into CO_2. As shown in Figure 9, the elongation of the C−O bonds increases with the increases of the net charges of chemisorbed CO_2 molecules. It indicates that stronger electron transfer from the surface into the antibonding orbital of CO_2 induces higher activation of the C−O bonds. On Ni(110), **12-5h** is the most negatively charged structure, which has two elongated C−O bonds (1.292 and 1.291 Å vs 1.171 Å). On Ni(100), the two most negatively charged structures are **7-2lb** and **5-3h**. In **7-2lb**, the elongated C−O bond lengths are 1.273 and 1.226 Å. In **5-3h**, the C−O bond lengths are 1.264 and

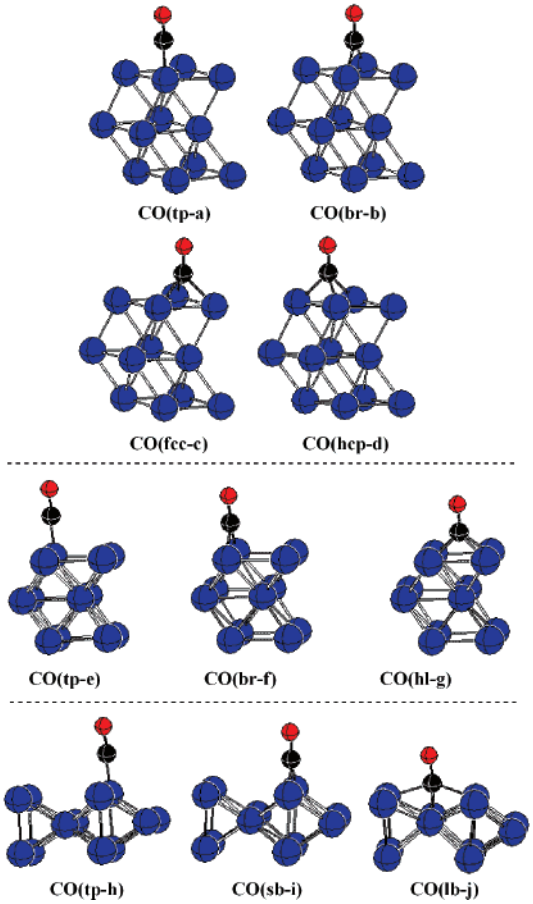

Figure 10. Structures of chemisorbed CO on nickel surfaces at $^1/_4$ ML coverage [**a**−**d** on Ni(111)/top, **e**−**g** on Ni(100)/middle, and **h**−**l** on Ni(110)/bottom].

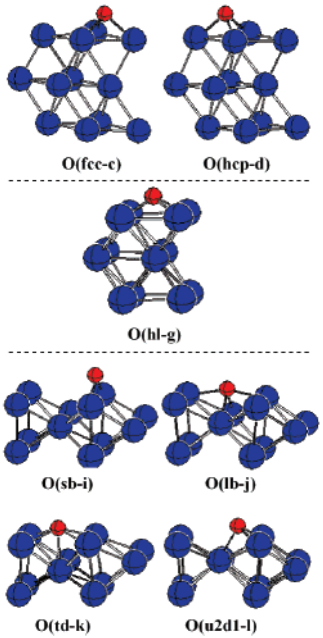

Figure 11. Structures of chemisorbed atomic O on nickel surfaces at $^1/_4$ ML coverage [**a**−**d** on Ni(111)/top, **e**−**g** on Ni(100)/middle, and **h**−**l** on Ni(110)/bottom].

1.257 Å. On Ni(111), the two most negatively charged structures are **3-4hf** and **4-5fcc**. In **3-4hf**, the C−O bonds are elongated to 1.261 and 1.255 Å, while the C−O bond lengths are 1.253 and 1.251 Å in **4-5fcc**. Comparatively, the C═O bond activation ability of nickel surfaces follows the sequence Ni(110) >

TABLE 4: Computed Chemisorption Energies (ΔE_{chem}, eV) and Structures (d, Å) as Well as the Net Charges (q) of CO and O on Ni Surfaces[a] at $^1/_4$ ML

	ΔE_{chem}[b]	d_{O-C}	d_{C-Ni} [d_{O-Ni}]	q	q_O	q_C
CO		1.144		0	−0.43	0.43
CO(tp-a)	−1.55	1.161	1.737	−0.15	−0.35	0.20
CO(br-b)	−1.79	1.181	1.869, 1.878	−0.35	−0.32	−0.03
CO(fcc-c)	−1.88	1.188	1.957, 1.957, 1.965	−0.39	−0.31	−0.08
CO(hcp-d)	−1.91	1.189	1.947, 1.949, 1.957	−0.41	−0.32	−0.09
CO(tp-e)	−1.72	1.162	1.739	−0.01	−0.01	0.00
CO(br-f)	−1.93	1.179	1.869, 1.882	−0.32	−0.33	0.01
CO(hl-g)	−2.04	1.207	2.019, 2.040, 2.045, 2.069	−0.52	−0.33	−0.19
CO(tp-h)	−1.75	1.163	1.732	−0.18	−0.37	0.19
CO(sb-i)	−1.94	1.180	1.861, 1.880	−0.33	−0.35	0.02
CO(lb-j)	−1.52	1.216	1.955, 2.022, 2.025, 2.048	−0.52	−0.36	−0.16
O(fcc-c)	−5.07		[1.853, 1.853, 1.854]	−0.55		
O(hcp-d)	−4.99		[1.850, 1.850, 1.850]	−0.55		
O(hl-g)	−5.45		[1.953, 1.953, 1.955, 1.956]	−0.62		
O(sb-i)	−4.85		[1.770, 1.771]	−0.54		
O(lb-j)	−4.62		[1.934, 1.935, 1.935, 1.937]	−0.59		
O(td-k)	−4.64		[2.047, 2.086, 2.086, 2.111, 2.112]	−0.64		
O(u2d1-l)	−4.85		[1.837, 1.838, 1.929]	−0.58		

[a] The label of the chemisorbed CO and O corresponds to the adsorption sites in Figure 1: **a**−**d** on Ni(111), **e**−**g** on Ni(100), and **h**−**l** on Ni(110). [b] The chemisorption energies of O were relative to atomic oxygen, i.e., $\Delta E_{chem}(O) = E(O/slab) - [E(O) + E(slab)]$.

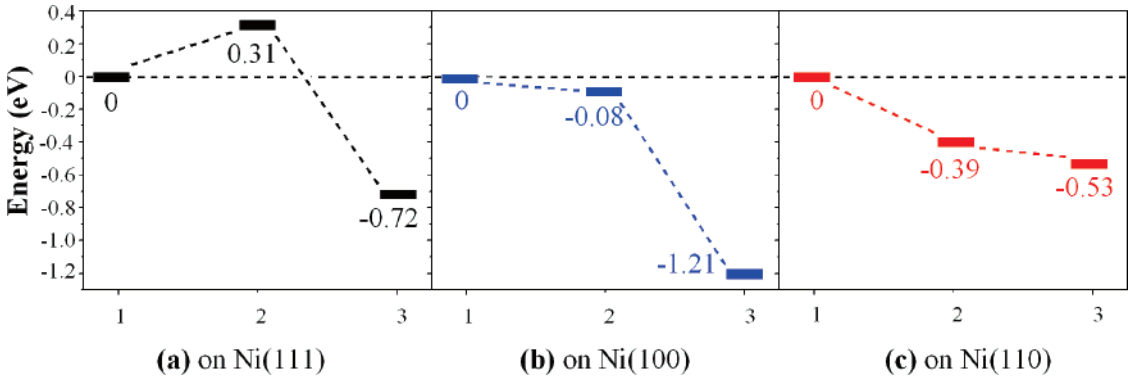

Figure 12. Thermodynamic scheme of dissociative chemisorption of CO_2 on nickel surfaces: 1 → 2 for CO_2 chemisorption; 2 → 3 for chemisorbed CO_2 dissociation.

Ni(100) > Ni(111). Since stronger electron transfer from the surface to chemisorbed CO_2 molecules induces higher CO_2 activation, it is proposed that the usage of Lewis basic additives on nickel catalysts can improve the CO_2 activation by improving the surface ability of presenting electrons.

From the computed chemisorption energies and C═O bond lengths, both the chemisorption ability of the nickel surfaces and the activation ability to C═O bonds are in the order Ni(110) > Ni(100) > Ni(111). The chemisorption energies on Ni(110) are negative, which means a strong chemisorption ability, and the C═O bonds are strongly activated, in agreement with the experimental result of dissociative chemisorption. On Ni(100), CO_2 chemisorption is almost thermally neutral and the C═O bonds are only moderately activated, and this agrees with the observation of both dissociative chemisorption and nondissociative adsorption. On Ni(111), the computed positive chemisorption energies of CO_2 and relatively weak C═O bond elongation indicate the chemisorption and activation of CO_2 on this surface to not be favored, in agreement with the low-temperature experiments for the nondissociative adsorption of CO_2 on Ni(111).

The main drawback in the Ni-catalyzed dry reforming of CH_4 is the poor stability of the catalysts mostly caused by carbon deposition. The accumulation of surface carbon comes from CH_4 dissociation and the Bouduard reaction ($2CO = C_{(ads)} + CO_2$) and is believed to be the main reason for carbon deposition.[1] Since Lewis basic materials can improve the activation of C−O bonds, they should also promote the CO_2 dissociation to CO and surface oxygen $O_{(ads)}$. In turn, the surface $O_{(ads)}$ can oxidize the surface $C_{(ads)}$ to CO. The combination of these two steps is the Bouduard back reaction ($C_{(ads)} + CO_2 = 2CO$). Therefore, usage of Lewis basic additives is an alternative way to hinder carbon deposition on nickel catalysts. This agrees with the experimental findings. Arena et al. found that alkali (Li, Na, K) additives alter the electronic properties of the active Ni phase, resulting in a strong inhibition of the Bouduard reaction in their experiments.[47]

(e) CO_2 Dissociative Chemisorption. To analyze the thermodynamics of CO_2 dissociative chemisorption on nickel surfaces, the chemisorption of CO and atomic oxygen was calculated at $^1/_4$ ML coverage. There are 10 stable structures for CO adsorption (Figure 10) and 7 for atomic oxygen (Figure 11). The computed chemisorption energies, structural parameters, and net charges of CO and atomic O are listed in Table 4.

From the chemisorption energies in Table 4, on Ni(111), CO prefers to locate on 3-fold hollow sites with chemisorption energies of −1.91 eV on the hcp site (**CO(hcp-d)**) and −1.88 eV on the fcc site (**CO(fcc-c)**). These agree with the previous theoretical values[48] of 1.90 and 1.87 eV calculated by using the PW91 functional in the Vienna ab initio simulation package (VASP), and compared to the experimental value 1.35 eV.[49] Atomic oxygen prefers to chemisorb on the 3-fold hollow fcc sites with chemisorption energies of −5.07 and −4.99 eV. On

Ni(100), both CO and O prefer to chemisorb on the hollow site (**CO(hl-g)** and **O(hl-g)**) with chemisorption energies of −2.04 and −5.45 eV, respectively. On Ni(110), CO prefers to chemisorb on the short-bridge site (**CO(sb-i)**) with a chemisorption energy of −1.94 eV, while O prefers the short-bridge (**O(sb-i)**) and 3-fold hollow sites formed by two first-layer Ni atoms and one second-layer Ni atom (**O(u2d1-l)**), and the chemisorption energies are equal to −4.85 eV.

The computed thermodynamic schemes of CO_2 chemisorption and dissociation on nickel surfaces are shown in Figure 12. It shows that the dissociation of CO_2 on Ni surfaces is exothermic by −1.03 eV on Ni(111), −1.13 eV on Ni(100), and −0.14 eV on Ni(110) relative to the chemisorbed states, indicating the process to be preferred thermodynamically. The dissociative chemisorption energies are −0.72 eV on Ni(111), −1.21 eV on Ni(100), and −0.53 eV on Ni(110) relative to the free states. It indicates that Ni(100) is the most preferred site for CO_2 dissociation under thermodynamic control, followed by Ni(111) and Ni(110). The more favored CO_2 dissociation on Ni(100) shows at the same time also the higher concentration of adsorbed atomic oxygen O(ads), which can oxidize the surface $C_{(ads)}$ to CO to hinder carbon deposition. Accordingly, for Ni-catalyzed dry reforming of methane, the catalyst of Ni(100) as the main metal surface structure has a higher ability to hinder carbon deposition than those of Ni(111) and Ni(110), from the point of view of thermodynamics.

Conclusions

Chemisorption of CO_2 on the Ni(111), Ni(100), and Ni(110) surfaces was investigated by using the generalized gradient approximation (GGA) and the Perdew−Burke−Ernzerhof (PBE) functional at the level of density functional theory. On the basis of the computed chemisorption energies, the ability of CO_2 chemisorption on the nickel surfaces is in the order Ni(110) > Ni(100) > Ni(111), in agreement with the experiment and with the relative intensities of the frontier orbitals of the three nickel surfaces. Furthermore, CO_2 chemisorption is exothermic on Ni(110) but endothermic on Ni(111), while it is thermally neutral on Ni(100). Compared to $^1/_6$ ML, no lateral interaction between the adsorbed CO_2 on all surfaces at $^1/_4$ ML is found, but strong repulsive interaction is found at $^1/_2$ ML.

On all surfaces, the chemisorbed CO_2 is partially negatively charged and has elongated C−O bond lengths and a bent CO_2 structure. This is due to the enhanced electron transfer from the nickel surface into the antibonding orbital of CO_2, and the stronger the electron transfer, the stronger the CO_2 activation. It is therefore proposed that increased basicity of the surfaces might improve the ability of CO_2 activation and in turn reduce the surface carbon deposition. It is in agreement with the experimental results of dry reforming of methane. The thermodynamic preference of CO_2 dissociative chemisorption shows the order Ni(100) > Ni(111) > Ni(110), and Ni(100) has a higher ability of carbon deposition restraint.

Acknowledgment. This work was supported by Chinese Academy of Science and the National Nature Foundation of China (nos. 20473111 and 20590361).

Supporting Information Available: Tables showing total energies. This material is available free of charge via the Internet at http://pubs.acs.org.

References and Notes

(1) Rostrup-Nielsen, J. R.; Sehested, J.; Nørskov, J. K. *Adv. Catal.* **2002**, *47*, 65.
(2) Bradford, M. C. J.; Vannice, M. A. *Catal. Rev.—Sci. Eng.* **1999**, *41*, 1.
(3) Bodrov, I. M.; Apel'baum, L. O. *Kinet. Katal.* **1967**, *8*, 326.
(4) Nakamura, J.; Aikawa, K.; Sato, K.; Uchijima, T. *Catal. Lett.* **1994**, *25*, 265.
(5) Erdöhelyi, A.; Cserényi, J.; Solymosi, F. *J. Catal.* **1993**, *141*, 287.
(6) Erdöhelyi, A.; Cserényi, J.; Papp, E.; Solymosi, F. *Appl. Catal., A* **1994**, *108*, 205.
(7) Rostrup-Nielsen, J. R.; Bak Hansen, J.-H. *J. Catal.* **1993**, *144*, 38.
(8) Wang, H.-Y.; Au, C.-T. *Catal. Lett.* **1996**, *38*, 77.
(9) Wang, H.-Y.; Au, C.-T. *Appl. Catal., A* **1997**, *155*, 239.
(10) Zhang, Z.; Verykios, X. E. *Catal. Lett.* **1996**, *38*, 175.
(11) Burghgraef, H.; Jansen, A. P. J.; van Santen, R. A. *J. Chem. Phys.* **1994**, *101*, 11012.
(12) Osaki, T.; Masuda, H.; Mori, T. *Catal. Lett.* **1994**, *29*, 33.
(13) Erdöhelyi, A.; Fodor, K.; Solymosi, F. *Stud. Surf. Sci. Catal.* **1997**, *107*, 525.
(14) Shustorovich, E.; Bell, A. T. *Surf. Sci.* **1992**, *268*, 397.
(15) Walter, K.; Buyevskaya, O. V.; Wolf, D.; Baerns, M. *Catal. Lett.* **1994**, *29*, 261.
(16) Qin, D.; Lapszewicz, J.; Jiang, X. *J. Catal.* **1996**, *159*, 140.
(17) Mark, M. F.; Maier, W. F. *Angew. Chem., Int. Ed. Engl.* **1994**, *33*, 1657.
(18) Lercher, J. A.; Bitter, J. H.; Hally, W.; Niessen, W.; Seshan, K. *Stud. Surf. Sci. Catal.* **1996**, *101*, 463.
(19) Osaki, T.; Horiuchi, T.; Suzuki, K.; Mori, T. *J. Chem. Soc., Faraday Trans.* **1996**, *92*, 1627.
(20) Bradford, M. C. J.; Vannice, M. A. *Appl. Catal., A* **1996**, *142*, 97.
(21) Bradford, M. C. J.; Vannice, M. A. *J. Catal.* **1998**, *173*, 157.
(22) Wang, S.-G.; Li, Y.-W.; Lu, J.-X.; He, M.-Y.; Jiao, H. *J. Mol. Struct. (THEOCHEM)* **2004**, *673*, 181.
(23) Garin, F.; Keller, V.; Ducros, R.; Muller, A.; Maire, G. *J. Catal.* **1997**, *166*, 136.
(24) Matsuo, Y.; Yoshinaga, Y.; Sekine, Y.; Tomishige, K.; Fujimoto, K. *Catal. Today* **2000**, *63*, 439.
(25) Matsui, N.; Anzai, K.; Akamatsu, N.; Nakagawa, K.; Ikenaga, N.; Suzuki, T. *Appl. Catal., A* **1999**, *179*, 247.
(26) Solymosi, F. *J. Mol. Catal.* **1991**, *65*, 337.
(27) Wambach, J.; Freund, H.-J. In *Carbon Dioxide Chemistry: Environmental Issues*; Paul, J., Pradier, C.-M., Eds.; Athenaeum Press: Cambridge, U.K., 1994; p 31.
(28) Freund, H. J.; Messmer, R. P. *Surf. Sci.* **1986**, *172*, 1.
(29) Dubois, L. H.; Somorjai, G. A. *Surf. Sci.* **1983**, *128*, L231.
(30) Freund, H. J.; Behner, H.; Bartos, B.; Wedler, G.; Kuhlenbeck, H.; Neumann, M. *Surf. Sci.* **1987**, *180*, 550.
(31) Choe, S. J.; Kang H. J.; Park D. H.; Huh D. S.; Park J. *Appl. Surf. Sci.* **2001**, *181*, 265.
(32) White, J. A.; Bird, D. M. *Phys. Rev. B* **1994**, *50*, 4954.
(33) Perdew, J. P.; Burke, K.; Ernzerhof, M. *Phys. Rev. Lett.* **1996**, *77*, 3865.
(34) (a) Payne, M. C.; Allan, D. C.; Arias, T. A.; Joannopoulos, J. D. *Rev. Mod. Phys.* **1992**, *64*, 1045. (b) Milman, V.; Winkler, B.; White, J. A.; Pickard, C. J.; Payne, M. C.; Akhmataskaya, E. V.; Nobes, R. H. *Int. J. Quantum Chem.* **2000**, *77*, 895.
(35) Vanderbilt, D. *Phys. Rev. B* **1990**, *41*, 7892.
(36) Monkhorst, H. J.; Pack, J. D. *Phys. Rev. B* **1976**, *13*, 5188.
(37) Louie, S. G.; Froyen, S.; Cohen, M. L. *Phys. Rev. B* **1982**, *26*, 1738.
(38) Nayak, S. K.; Nooijen, M.; Bernasek, S. L.; Blaha P. *J. Phys. Chem. B* **2001**, *105*, 164.
(39) Cheng, H.; Reiser, D. B.; Dean, S. W., Jr.; Baumert, K. *J. Phys. Chem. B* **2001**, *105*, 12547.
(40) Ge, Q.; Jenkins, S. J.; King, D. A. *Chem. Phys. Lett.* **2000**, *327*, 125.
(41) Ge, Q.; Neurock, M.; Wright, H. A.; Srinivasan, N. *J. Phys. Chem. B* **2002**, *106*, 2826.
(42) Cao, D.-B.; Zhang, F.-Q.; Li, Y.-W.; Jiao, H. *J. Phys. Chem. B* **2004**, *108*, 9094.
(43) Henry, C. R. *Surf. Sci. Rep.* **1998**, *31*, 235.
(44) Bengaard, H. S.; Alstrup, I.; Chorkendorff, I.; Ullmann, S.; Rostrup-Nielsen, J. R.; Nørskov, J. K. *J. Catal.* **1999**, *187*, 238.
(45) Ciobîcă, I. M.; Frechard, F.; van Santen, R. A.; Kleyn, A. W.; Hafner, J. *J. Phys. Chem. B* **2000**, *104*, 3364.
(46) Ledentu, V.; Dong, W.; Sautet, P. *J. Am. Chem. Soc.* **2000**, *122*, 1796.
(47) Arena, F.; Frusteri, F.; Parmaliana, A. *Appl. Catal., A* **1999**, *187*, 127.
(48) Shah, V.; Li, T.; Baumert, K. L.; Cheng, H.; Sholl, D. S. *Surf. Sci.* **2003**, *537*, 217.
(49) Stuckless, J. T.; Ai-Sarraf, N.; Wartnaby, C.; King, D. A. *J. Chem. Phys.* **1993**, *99*, 2202.